Band bending and k-resolved band offsets at the $HfO_2/n^+(p^+)$Si interfaces explored with synchrotron-radiation ARPES/XPS

L. L. Lev [1,2,3,*] V. N. Strocov [2,†] Y. Y. Lebedinskii,[1] T. Schmitt,[2] and A. V. Zenkevich [1,‡]

[1]*Moscow Institute of Physics and Technology, 9, Institutskiy lane, Dolgoprudny, Moscow region, 141700, Russia*

[2]*Swiss Light Source, Paul Scherrer Institute, 5232 Villigen-PSI, Switzerland*

[3]*P. N. Lebedev Physical Institute of the Russian Academy of Sciences, 53 Leninskiy Prospekt, 119991 Moscow, Russia*

(Received 15 April 2022; revised 28 July 2022; accepted 8 August 2022; published 30 August 2022)

HfO_2/Si interface is among the most studied heterostructure materials due to the use of HfO_2 in the mainstream Si microelectronic technology. Following the discovery of new functionalities in HfO_2 such as ferroelectric and reversible resistance-switching properties, we study ultrathin HfO_2 films grown on highly doped (p^+ and n^+) Si by means of synchrotron-based soft-x-ray spectroscopy techniques, such as x-ray photoelectron spectrosopy (XPS) and angle resolved photoelectron spectroscopy (ARPES). With angular resolution, we directly obtain the electronic dispersions $E(\mathbf{k})$ of the single-crystalline Si substrate in contact with the HfO_2 overlayer, depending on the Si doping and heat treatment, and determine the **k**-resolved band offset at the interface. Analysis of the Hf and Si core-level energies and line shapes as a function of photon energy yields band bending in HfO_2 and Si. The evolution of the Hf 4f linewidth upon annealing points to development of a potential distribution across HfO_2 due to charged defects at the surface and interface with Si. The effect of intense x-ray beam on the HfO_2/Si interfaces, distorting their pristine electronic structure, is evaluated from the time evolution of line shape and position under irradiation. We propose a model explaining the effects of both heat treatment and x-ray irradiation on the HfO_2/Si electronic structure in terms of oxygen vacancies generated at the surface of HfO_2 and its interface to Si, where the released O atoms react with Si to form SiO_x at the interface. The knowledge of the irradiation-dependent band bending is essential for precise determination of the **k**-dependent band offset locally at the HfO_2/Si interface.

DOI: 10.1103/PhysRevMaterials.6.084605

I. INTRODUCTION

Over the last two decades, thin-film HfO_2 has been one of the most studied transition-metal oxides. HfO_2 combines a large band gap E_g of 5.6–5.8 eV, high dielectric permittivity $\kappa_{HfO_2} = 16$–25, high thermal stability (melting point $T_{melt} \approx 2780^\circ$C), high thermodynamic stability in contact with Si, and high energy barriers for electrons and holes with respect to Si 2.0 and 2.5 eV, respectively (see Ref. [1] and references therein). In the early 2000s, high-κ HfO_2 was identified as the best gate dielectric material to substitute SiON in complementary metal-oxide-semiconductor (CMOS) field-effect transistors (FETs) [2]. The subsequent discovery of ferroelectric properties in doped or alloyed HfO_2 [3] ignited an explosive interest in this material due to the prospects of development of CMOS-compatible nonvolatile memory devices, such as ferroelectric FETs [4,5] or ferroelectric tunnel junction employing Si as a (bottom) electrode [6–8]. Alternatively, ultrathin ferroelectric HfO_2 exhibiting a negative capacitance effect can be utilized in ultralow-power FETs [9]. In addition, HfO_2 has been found a promising candidate for the nonvolatile resistive random access memory [10,11]. Furthermore, this material may replace Si oxide in flash memory devices [12].

However, despite numerous theoretical and experimental studies of the chemical and electronic structure of the HfO_2/Si interface (e.g., Refs. [13–18]), which is at the core of the modern metal-oxide-semiconductor field-effect transistor technology and plays a crucial role in emerging ferroelectric memory and logic device concepts, there are still issues worth to be addressed. In particular, to the best of our knowledge, the electron momentum **k**-resolved electronic band structure $E(\mathbf{k})$ of doped monocrystalline Si in contact with thin-film HfO_2 has so far not been experimentally observed. Also, charged defects in HfO_2, predominantly oxygen vacancies (V_O) often generated at the interface with Si, should affect the interfacial band offset. Furthermore, the evolution of electronic structure of HfO_2/Si interface as a function of Si doping and heat treatment still stays largely unknown. The whole body of such a detailed information would be highly useful for the implementation of emerging electronic devices employing thin-film HfO_2 on Si as their functional basis.

(Angle-integrated) x-ray photoelectron spectroscopy (XPS) is a classical technique to elucidate the chemical properties in a subsurface layer. It has also been often used to gain information on the band offset at the dielectric/semiconductor interface [19] which is instrumental to predict and model the electrical properties in the devices based on MOS structures. Previously, most XPS analyses

*lll_ru@mail.ru
†vladimir.strocov@psi.ch
‡zenkevich.av@mipt.ru

of the HfO_2/Si junctions [16,20–24] were performed with laboratory setups, where the photon energy ($h\nu$) was fixed, and the x-ray brightness on the sample was limited by x-ray tubes and focusing optics.

Nevertheless, even with such relatively low flux, various authors reported irradiation-induced shifts of the spectral features, which led to discrepancies in the measured band offsets (see, e.g., Ref. [20] and references therein). This phenomenon was interpreted based on the so-called "differential charging model." According to this model, during the x-ray irradiation the photoelectrons emitted from the oxide dielectric cannot be compensated by electrons from the grounded sample holder so that it would rather discharge into the semiconductor underlayer. As a result, the induced positive charges give rise to the electrical field causing a band bending at the oxide/semiconductor interface. Consequently, in order to get consistent values of the valence-band (VB) offsets, such intrinsic charging effects in the dielectric/semiconductor stack have to be taken into account [20,21]. However, over the years a wealth of observations has built up that such phenomena caused by the escape of the photoelectrons cannot explain the whole complex physicochemical processes at the interface. In particular, the radiation induces oxidation of Si in contact with HfO_2 followed by the formation and charging of oxygen vacancies. These effects of intense x-ray irradiation required further comprehensive studies.

Modern synchrotron-based XPS instruments deliver a several orders of magnitude higher x-ray brightness on the sample as well as a 3–4 times better energy resolution compared to the laboratory setups. Although such parameters are certainly a big advantage in terms of sensitivity, energy resolution, and data acquiring time, the irradiation effects in the dielectric/semiconductor samples are expected to become much stronger.

Angle-resolved photoelectron spectroscopy (ARPES) is a unique experimental technique to directly determine **k**-resolved band structure of crystalline solids $E(\mathbf{k})$ [25]. The use of synchrotron radiation adds, besides high x-ray brightness and energy resolution, variable photon energies allowing precise navigation in three-dimensional **k**-space and tunability of the probing depth determined by kinetic energy of photoelectrons. Pushing the ARPES experiment into the soft-x-ray photon-energy range (SX-ARPES) increases the probing depth by a factor of 3–5 compared to the conventional experiments in the vacuum ultraviolet (VUV) range, allowing thereby access to buried interfaces and heterostructures which are in the heart of electronic devices [26,27]. Such applications of SX-ARPES have previously been demonstrated for various semiconductor, oxide, and hybrid heterostructures (see, e.g., Refs. [26,28–32].

In this work, we use SX-ARPES for a detailed study of the interface between ultrathin HfO_2 films, grown by atomic layer deposition (ALD) technique, and highly doped Si(001) substrates. We directly measure $E(\mathbf{k})$ of the Si substrates aligned with the HfO_2 overlayer for HfO_2/p^+Si and HfO_2/n^+Si interfaces as well as evaluate band bending in HfO_2 and Si. We elucidate not only the role of the doping of Si on the interfacial band structure, but also the effect of (*in situ*) annealing of HfO_2/Si samples. Furthermore, we determine the effects of high-intensity soft x-ray radiation on the local electric fields at the interface as reflected by the time evolution of the core-level spectra under irradiation. These irradiation effects were used as an additional tool to elucidate the distribution of (charged) defects in HfO_2 in contact with the highly doped Si. The observed temporal evolution of the Hf $4f$ spectral features in HfO_2 is explained in terms of the generation and charging of oxygen vacancies in HfO_2 and concomitant oxidation of Si at the $HfO_2/p^+(n^+)$Si interface. The revealed fundamental electronic properties of the HfO_2/Si interfaces will serve as a solid ground for development of advanced electronic devices based on these materials.

II. EXPERIMENT PROCEDURE

Amorphous HfO_2 layers of 3 nm in thickness were grown by the ALD technique (ALD reactor Sunale R-100 Picosun OY) at $T = 240$°C using $Hf[N(CH_3)(C_2H_5)]_4$ and H_2O as precursors and N_2 as carrier and purging gas on the highly doped p^+Si and n^+Si substrates ($\rho = 0.005\,\Omega$ cm, $N_D \sim 10^{20}\,cm^{-3}$). At such a doping level Si exhibits a metallic behavior in a wide temperature range [33]. Native SiO_2 layer was removed using standard cleaning procedure (in a 10% HF (hydrofluoric acid) solution for 15 s), its absence prior to the HfO_2 ALD growth confirmed by *in situ* laboratory XPS analysis coupled with the reactor (Fig. S1 in Ref. [34]). As-grown HfO_2/Si samples were immediately put in the desiccator under vacuum and opened before loading to the sample holder at the synchrotron. Annealing of the samples was performed *in situ* at a temperature of $T = 400$°C.

The experiments were performed at the SX-ARPES endstation [27] of the ADvanced RESonant Spectroscopies (ADRESS) beamline [26] of the Swiss Light Source. The use of SX-ARPES with larger probing depth compared to the conventional VUV range was critical for the analysis of the buried HfO_2/Si interface. A high photon flux of about 10^{13} photons/s/(0.01%BW)$^{-1}$ was essential for our experiments in the soft x-ray range with $h\nu = 280$–1500 eV, where the photoexcitation cross section of the valence states becomes extremely small [35]. The photon beam was focused to a spot of $\sim 30 \times 75\,\mu m^2$ on the sample surface. In order to maximize the coherent spectral fraction, reduced by the thermal atomic motion [36], the measurements were performed at $T = 12$ K. The combined (beamline and analyzer) energy resolution varied from 60 meV for $h\nu = 350$ to 270 meV for $h\nu = 1400$ eV, and the analyzer angular resolution was $\sim 0.1°$. The experiment geometry and other relevant details of our SX-ARPES experiment have been reported elsewhere [29].

III. RESULTS AND DISCUSSION

A. ARPES data on the *k*-dependent band offset

We will now analyze the ARPES data on HfO_2/Si as a function of $h\nu$, which controls the out-of-plane electron momentum k_z in the crystalline Si (the conversion formulas for our experimental geometry, including the photon-momentum correction, are compiled in Ref. [27]). These data for the HfO_2/n^+Si sample, rendered into an out-of-plane iso-E_B map in (k_x, k_z) coordinates in the $X\Gamma W$ plane of the bulk Brillouin zone (BZ) of Si [Fig. 1(a)] with an inner potential V_0 of 10 eV, are displayed in Fig. 1(b). The white dashed line correspond-

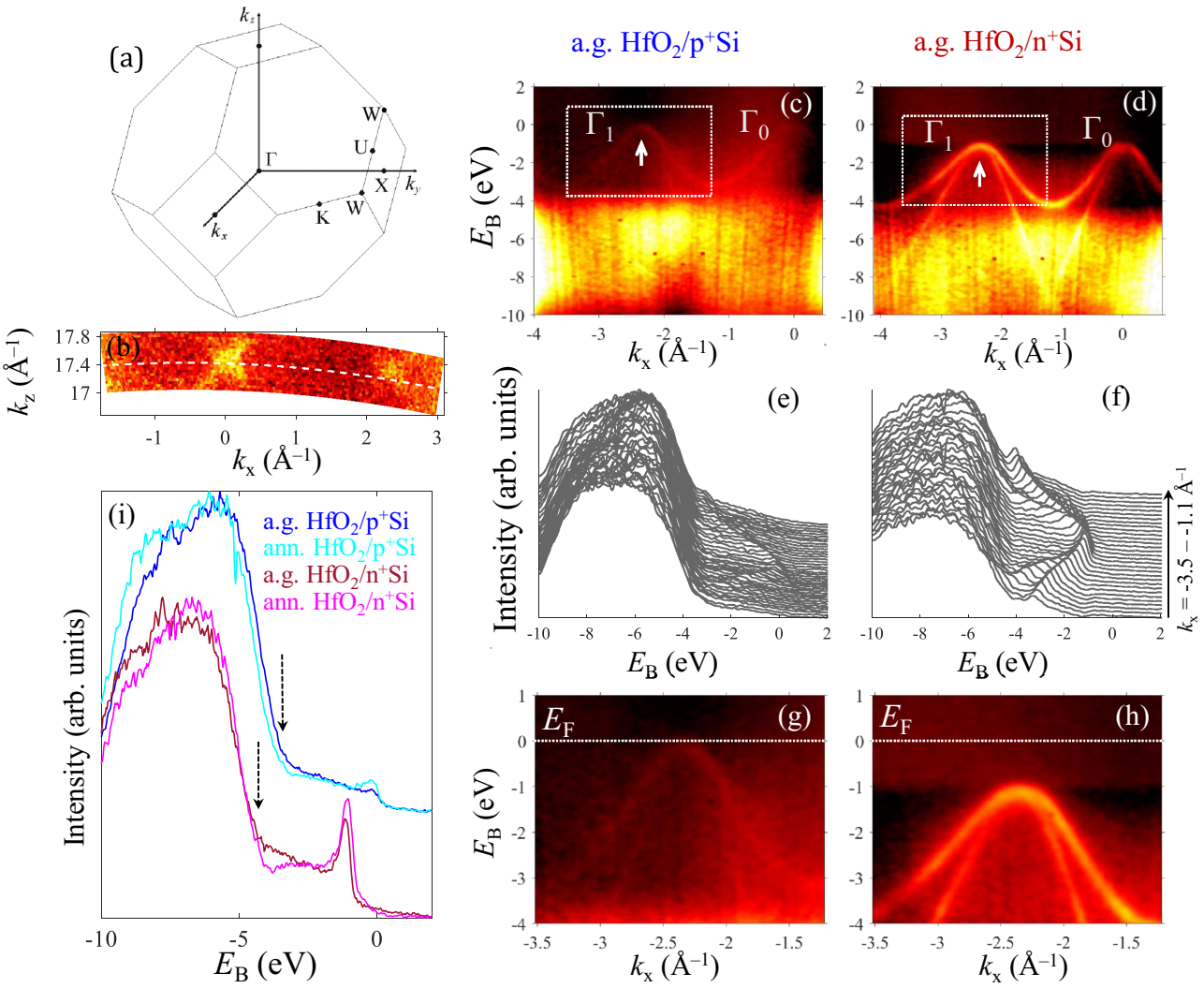

FIG. 1. (a) Bulk BZ of Si. (b) $h\nu$-dependent ARPES data for the HfO_2/n^+Si sample rendered into out-of-plane iso-E_B maps in the $X\Gamma X$ plane of the bulk BZ of Si at $E_B = 1.0$ eV below the VB maximum (VBM) measured for $h\nu = 1070$–1170 eV. The white dashed line corresponds to $h\nu = 1120$ eV. ARPES dispersions for the HfO_2/p^+Si (c) and HfO_2/n^+Si (d) as-grown samples along the Γ-X directions of the bulk BZ ($h\nu = 1120$ eV). The observed band dispersions were insensitive to the annealing. (e), (f) EDC spectra around the Γ_1 point extracted from (c) and (d), respectively. (g), (h) Enlarged ARPES dispersions taken from the region around Γ_1 as marked by rectangles in (c) and (d). (i) Valence-band EDC spectra extracted from (c), (d) at the Γ_1 point marked by the white arrow, for the as-grown (a.g.) and annealed (ann.) HfO_2/p^+Si and HfO_2/n^+Si samples. VBMs for HfO_2 are marked with arrows.

ing to $h\nu = 1120$ eV crosses the VB maximum (VBM) of the 3D band structure of Si in the Γ point. All ARPES data in Figs. 1(c)–1(i) are measured at this photon energy. The photoelectron inelastic mean-free path (IMFP) λ_{PE} for this energy, calculated with the well-established predictive Tanuma, and Powell and Penn (TPP-2M) equation [37], is about 26.8 Å. Consequently, the intrinsic resolution in k_z, which is expressed by $\Delta k_z = 1/\lambda_{PE}$ [38], is approximately equal to 0.04 Å. This value, corresponding to ∼3.4% of the BZ, is sharp enough that we neglect its effect in the present study.

The ARPES images $I_{PE}(E_B, k_x)$ of the Si band structure for the as-grown HfO_2/p^+Si and HfO_2/n^+Si samples are shown in Figs. 1(c) and 1(d), respectively. For all spectra, the nondispersive spectral fraction is suppressed by subtracting angle-integrated spectral intensity, which overwhelms the raw spectra, see Fig. S2 in Ref. [34]. Figures 1(e) and 1(f) show the energy distribution curve (EDC) spectra for k_x at the Γ point obtained from Figs. 1(c) and 1(d), and Figs. 1(g), (h) zoom in the ARPES images near this point. The spectra are referred to the Fermi level (E_F) of the golden foil in electrical contact with the sample. The broad nondispersive band in a binding energy (E_B) interval of −4–−10 eV corresponds to the O $2p$ and Hf $5d$ states in HfO_2's VB. In the HfO_2 band gap at $E_B = -0$– − 4 eV, one can discern dispersive states coming from the buried Si, where the heavy and light/spin-orbit split hole bands can be readily identified. The spectral weight of the Si bands in the HfO_2/p^+Si sample is much lower compared to the HfO_2/n^+Si one. Tentatively, this difference can trace back to the strong band bending in Si in the former (for more details see Supplemental Material [34], Sec. I). The ARPES spectra measured after the sample annealing (not shown here for brevity) did not show any notable changes in the band dispersions but only energy shifts discussed below.

TABLE I. VB offsets locally at the $HfO_2/p^+(n^+)$Si interfaces before and after corrections for band bending as well as for the irradiation effect.

Sample	Before correction	After band-bending correction	After correction of the temporal effect: Bulk	After correction of the temporal effect: Interface
As-grown HfO_2/p^+Si	3.39 ± 0.09	3.44 ± 0.09	3.09 ± 0.09	3.00 ± 0.15
Annealed HfO_2/p^+Si	3.55 ± 0.09	3.56 ± 0.09	3.00 ± 0.09	3.68 ± 0.14
As-grown HfO_2/n^+Si	3.32 ± 0.07	3.33 ± 0.07	3.78 ± 0.09	2.67 ± 0.11
Annealed HfO_2/n^+Si	3.40 ± 0.07	3.48 ± 0.07	3.82 ± 0.07	3.21 ± 0.11

In order to quantitatively determine the band alignment of the VB states of HfO_2 with respect to those of Si, in Fig. 1(i) we plot the EDC spectra $I(E_B)$ derived from the above $I_{PE}(E_B, k_x)$ corresponding to VBM of Si in the Γ point at the in-plane momentum $k_{||} = 0$ (white arrows in Figs. 1(c) and 1(d)). This plot includes data for both as-grown and annealed samples. The small peak, corresponding to the top of the VBM of Si, is located near E_F, while the upper edge of HfO_2's VB is at $E_B \sim -4$ eV. At this point we stress that the correct determination of the VB offsets must invoke the VBM of Si in the Γ point of its three-dimensional band structure, which is achieved only: (1) at particular photon energies, corresponding to $k_\perp = 0$, and such experiments require therefore tunable synchrotron radiation; and (2) using the **k**-resolved coherent spectral fraction rather than the **k**-averaged one, which rapidly builds up with temperature and represents essentially the density of states [36]. Such experiments require cooling down the samples to temperatures below few tens of K. Our methodological approach is more accurate than the common determination of the VBM from the spectral leading edge, in particular because the latter varies with $h\nu$ due to varying $k_\perp$ and photoexcitation matrix elements.

Using the methodology illustrated in Fig. S3 in Ref. [34], we can derive the VB offsets between HfO_2 and Si locally at their interface for both as-grown and annealed HfO_2/p^+Si and HfO_2/n^+Si samples by comparing the leading edge of the nondispersive HfO_2 states with the VBM of the dispersive Si states in the Γ point. The obtained VB offsets given in Table I (left column) look close for HfO_2/n^+Si and HfO_2/p^+Si interfaces. Since the Fermi levels p^+Si and n^+Si substrates are shifted by ∼1 eV, so are the VB edges of both Si and HfO_2 for both as-grown and annealed samples [Fig. 1(i)]. We note that these values are "averaged" in the sense that they are obtained without taking into account the band bending, which will be further considered below.

B. Core-level spectra: Band bending in HfO_2 and Si

Figure 2 displays Si $2p$ [Fig. 2(a)] and Hf $4f$ [Fig. 2(b)] core-level spectra for the as-grown and *in situ* annealed HfO_2/p^+Si and HfO_2/n^+Si samples. The Si $2p$ spectrum is a doublet with the spin-orbit splitting $\Delta E_B \approx 0.62$ eV. The depth of the dip between the two components of the doublet [Fig. 2(a), inset)] qualitatively informs about their energy broadening. It decreases when going from the HfO_2/p^+Si sample to the HfO_2/n^+Si one and with annealing of the samples. The broadening becomes more pronounced for lower photon energies implying smaller probing depth (as described in more detail in the Supplemental Material [34], Fig. S4 and the related discussion in Sec. I), where Si $2p$ doublet cannot even be resolved [see Fig. S4(a), left panel]. In addition, these spectra contain a small broad peak at $E_B \approx -101.5$ eV, revealing the presence of SiO_2 presumably formed at the HfO_2/Si interface. As shown below, this oxidized Si emerges upon annealing and/or under x-ray irradiation. The observed broadening of Si $2p$ peak, particularly strong for the as-grown p^+Si sample, is the direct evidence of the band bending in Si (the "formally" derived Si $2p$ and Hf $4f$ linewidths are compiled in Table S1). We argue that the root cause for such band bending are charged defects on the HfO_2 side as will be discussed below.

Moreover, from Fig. 2(b), inset and Table S1 one can see that the broadening of the Hf $4f$ core-level spectra behaves oppositely to the Si $2p$ ones, i.e., the decrease of the Si $2p$ linewidth across the sample series is accompanied by the increase of that of the Hf $4f$ line. This observation points to an increase of the potential difference across HfO_2 layer presumably due to the generation and build-up of charged defects at the surface and/or the HfO_2/Si interface. The generation of defects, their charging, and the redistribution of these charges in HfO_2 gives rise to the change in the electronic band alignment at the interface linked to the band bending in Si manifested in the Si $2p$ core-level evolution discussed above. We note that, unlike the Si $2p$ spectra, the Hf $4f$ ones show no or negligible $h\nu$ dependence (see Fig. S4(b) in Ref. [34]). We also acquired the O $1s$ spectra (Fig. S5 in Ref. [34]) for all samples, and they have exhibited the same features as those observed for the Hf $4f$ and Hf $5d$ ones.

Our fitting procedure included the whole set of the experimental Hf $4f$ and Si $2p$ spectra [the details are described in the Supplemental Material [34], Sec. II and illustrated in Figs. 2(c) and 2(d)]. As the baselines for the core-level spectra, we chose the narrowest spectra which are the as-grown (a.g.) HfO_2/p^+Si spectrum for Hf $4f$ and the annealed (ann.) HfO_2/n^+Si one for Si $2p$. By fitting them with a superposition of the lines attributed to the series of sublayers, it is possible to reconstruct the potential profile $V(z)$ across the HfO_2/Si interface. The interfacial band alignment as well as the band bending in HfO_2 and Si are defined by charges in the heterostructure, and that should be taken into account to find an appropriate model for $V(z)$. For HfO_2 in contact with Si, it is well established [1,14,15] that oxygen vacancies (V_Os) can be formed in HfO_2. As it was shown previously by Robertson [39], the generation of V_Os in HfO_2 is strongly favored by its interfacing to Si, when the energy released from the reaction between the unbound O ions and Si atoms at the interface to form SiO_x can effectively promote further formation of V_Os. The electric dipole at the interface is formed when negatively

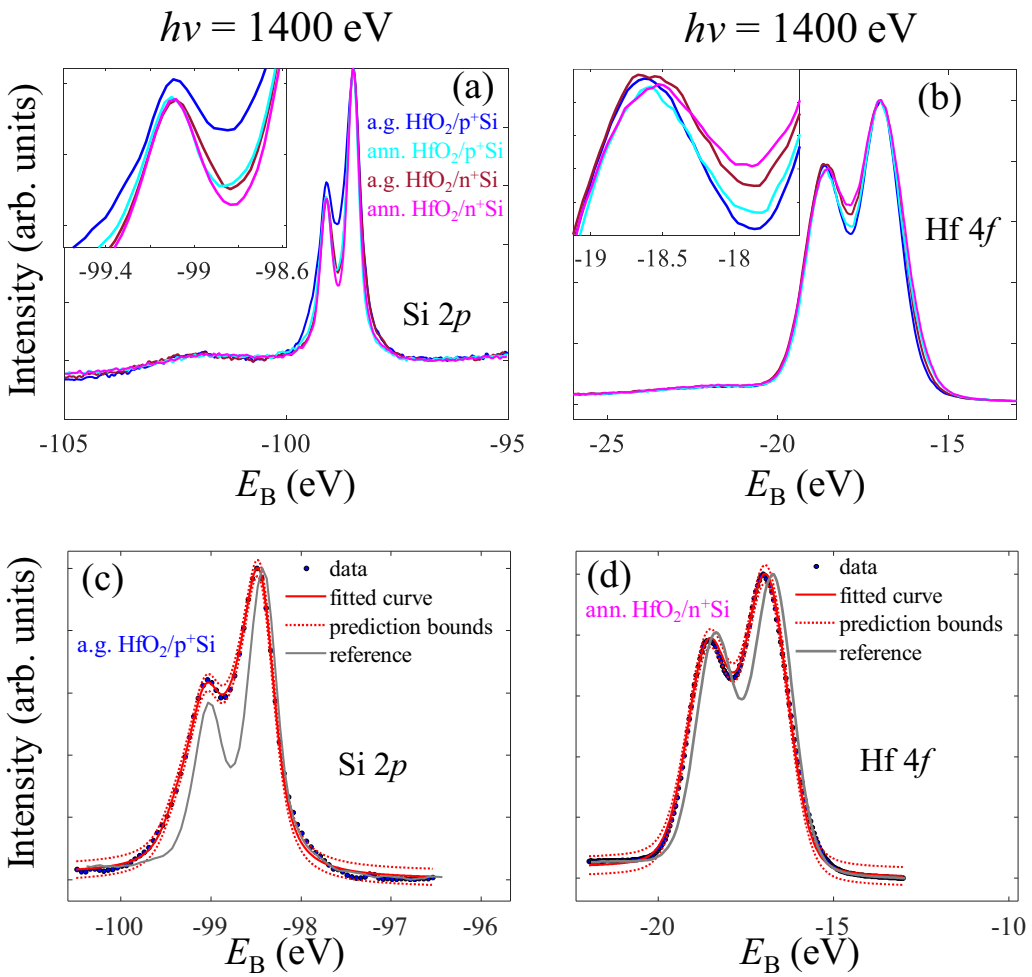

FIG. 2. (a) Si $2p$ core-level spectra for the annealed and as-grown HfO_2/p^+Si and HfO_2/n^+Si samples. (b) Hf $4f$ spectra for the same samples. In order to follow the peak broadening, the spectra are aligned at the peak maxima. The insets on both panels show dip between peaks in enlarged scale. (c), (d) An example of the potential profile-fitting procedure: (c) the measured Si $2p$ peak from a.g. HfO_2/p^+Si sample (dots) and the fitted profile (red), the prediction bounds (red dots) and the reference spectrum for the ann. HfO_2/n^+Si sample (gray); (d) the same for the Hf $4f$ peak with the reference spectrum for the a.g. HfO_2/p^+Si sample (gray).

charged O ions are transferred across the interface from HfO_2 to SiO_2, leaving positively charged O vacancies in HfO_2. V_Os can be also generated at the surface of HfO_2, especially during ultrahigh-vacuum annealing, ultimately leading to the effective "metallization" of the HfO_2 surface at the atomic scale [40].

Therefore, assuming that charges in the ultrathin HfO_2 layer are located at its surface and/or interface with Si, we can adopt a linear dependence for $V(z)$ across the layer. In the doped Si, the charged centers (dopant atoms) are uniformly distributed through the depth. Therefore, $V(z)$ in Si in the vicinity of its interface with HfO_2 can be approximated by a parabolic function [41]. The full $V(z)$ through the HfO_2/Si heterostructure will then be given by

$$V(z) = V_0^{HfO_2} z/a, \quad -a < z < 0$$

for HfO_2,

$$V(z) = \begin{cases} V_0^{Si}(z - z_0)^2/z_0^2, & 0 < z < z_0 \\ 0, & z \geqslant z_0 \end{cases}$$

for Si, where V_0^{Si} is the electrostatic potential at the Si interface relative to the bulk and $V_0^{HfO_2} = V(0) - V(-a)$ (potential drop), $a(= 3\,\text{nm})$ the thickness of the HfO_2 layer, and $z_0 = \sqrt{\frac{2\varepsilon_{Si}\varepsilon_0}{eN_D}} V_0^{Si}$ the width of the depletion layer. To connect this $V(z)$ with our experimental data, we modeled the Si $2p$ and Hf $4f$ lines within the approach previously used in Ref. [7], where the photoemission intensity was described as

$$I_{PE}(E_B) = \sum_i e^{-z_i/\lambda_{PE}} I_{PE}^{(i)}[E_B - V(z_i)],$$

where i enumerates the atomic layers; λ_{PE} is the IMFP calculated using the TTP-2M software [37]. The fitting parameters in this model were $V_0^{HfO_2}$, V_0^{Si}, and E_B (the latter had to be adjusted since $h\nu$ values in our experiment were not exactly calibrated). A value $\varepsilon_{Si} = 30$ of the permittivity, which is a constant parameter in the formula for z_0, is consistent with the ε_{Si} vs N_D dependence for the doped Si [42]. As the reference spectrum for fitting Si $2p$ data we use the narrowest spectrum found for the annealed HfO_2/n^+Si sample (gray) and for Hf

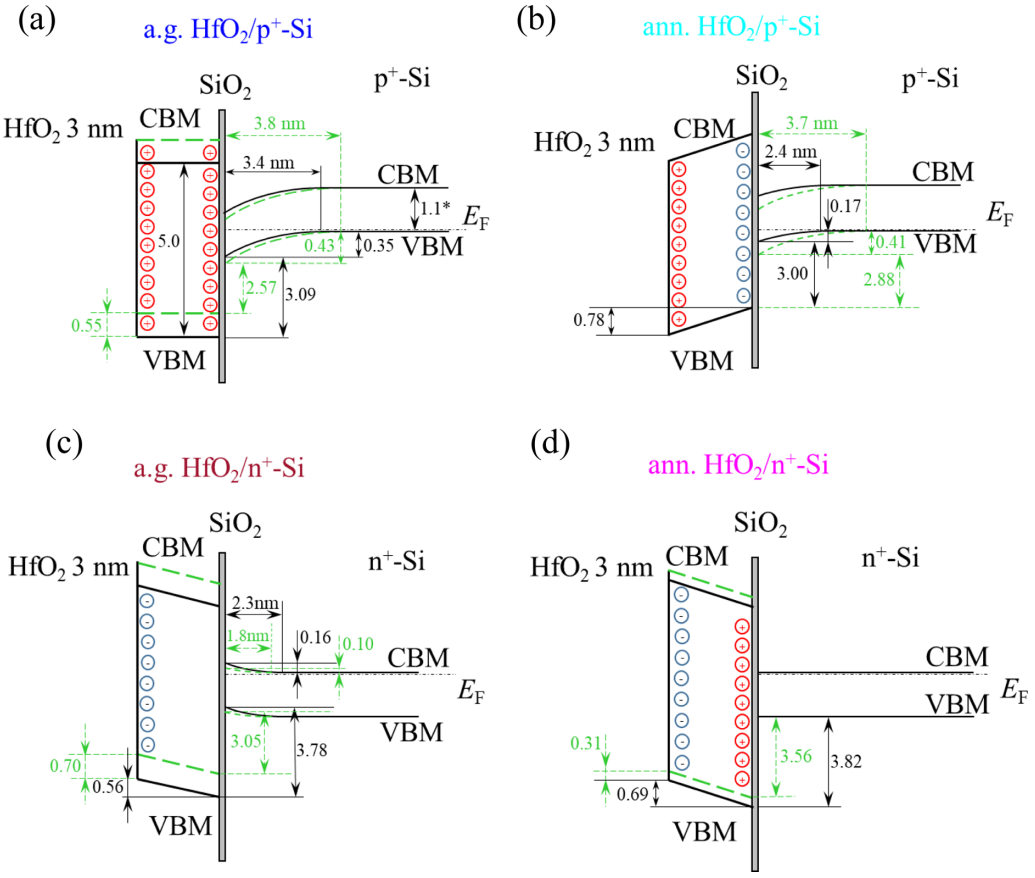

FIG. 3. Reconstructed band diagrams for different HfO_2/Si interfaces, at the beginning of x-ray irradiation (green) and upon saturation (black).

$4f$ data we use that for the as-grown HfO_2/p^+Si. For more details see Supplemental Material [34], Sec. I.

The resulting quantitative band diagrams across the HfO_2/Si stack for both n- and p doping as well as for as-grown vs annealed samples are given in Fig. 3. The shifts of the Hf $4f$ and Si $2p$ spectral lines with respect to their flat-band positions, obtained from the fitting, were used to correct the above VB offset values between the Γ point in Si and the VBM of HfO_2 from Table I for the band bending. These corrected offsets directly at the interface are also included in Table I.

C. Time evolution under x-ray irradiation

It should be noted that intense x-ray irradiation significantly changes the electronic structure of HfO_2/Si interfaces, which is manifested by energy shifts and broadening of both core-level and VB spectra. Whereas all spectra discussed above have been acquired after x-ray irradiation long enough to achieve saturation, here we will analyze time evolution of the VB, Si $2p$, and Hf $5p$ spectral lines under irradiation. This will allow us to better understand the interplay of the radiation-induced defects with charge-redistribution phenomena at the HfO_2/Si interfaces, because the energy position and the linewidth of the Hf $4f$ and Si $2p$ peaks reflect the band bending on the HfO_2 and Si sides, respectively. The time-evolution data were acquired with the same beamline settings as used for the previous measurements in saturation, namely, delivering a photon density of $\sim 10^{10}$ photons/s/μm^2 for the VB and Si $2p$ measurements, and $\sim 4 \times 10^9$ for Hf $5p$.

As an example, Figs. 4(a)–4(c) show representative spectra for the as-grown and annealed HfO_2/p^+Si samples measured at an irradiation time of almost zero, "pristine" state, and upon 1600 s. (The actual acquisition time for a pristine spectrum is 15 s.) In general, the spectra undergo significant evolution towards 800 s (for brevity not included in the figure) and then virtually saturate. Importantly, for all samples the annealing greatly reduces their irradiation sensitivity. A particularly dramatic time evolution can be seen in the Si $2p$ line of the as-grown HfO_2/p^+Si sample [Fig. 4(c)]: Whereas for the pristine spectrum the broadening of this line, induced by the band bending due to the interfacial charge, is so significant that the doublet cannot even be resolved, the line markedly sharpens under the irradiation, manifesting that the band bending in Si flattens.

An important observation for a.g. HfO_2/p^+Si samples is that while the pristine Si $2p$ spectrum has only a marginal spectral weight at $E_B \approx -101.5$ eV attributed to different Si oxides, this weight scales up upon x-ray irradiation for ~25 min until it saturates [see Fig. 4(c) and Fig. S6(b) in Ref. [34], respectively). In line with the idea that the creation of V_Os in HfO_2 is favored by its proximity to Si [39], we conjecture that in our case x rays generate the V_Os in HfO_2 near its

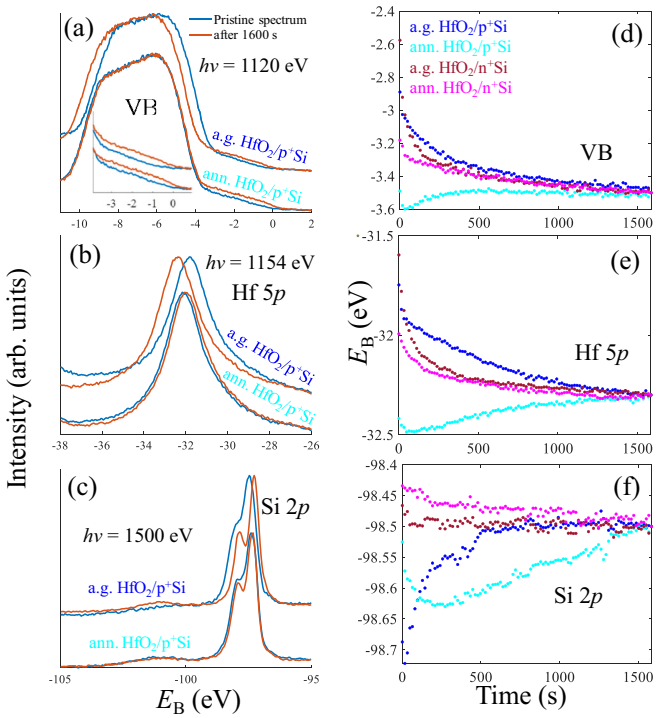

FIG. 4. Time evolution of the XPS spectra (photon energies indicated): (a) VB for the a.g. and ann. HfO_2/p^+Si samples. The inset shows a zoom in of the band-gap region of the spectra shifted in energy to match at the VB leading edge. (b) Hf $5p$ and (c) Si $2p$ spectra for the a.g. HfO_2/p^+Si and HfO_2/n^+Si sample. (d)–(f) Time evolution of the VB leading edge, Hf $5p$ and Si $2p$ peak energies for different samples.

interface with Si, and the released O ions react with Si to form SiO_x at the interface. As mentioned above, this process affects the charge distribution and eventually the band offset at the HfO_2/Si interface. From the peak areas attributed to Si^{4+} and Si^0 in the Si $2p$ spectra, using the standard procedure which takes into account the IMFP of photoelectrons in Si and SiO_2 [37,43], we evaluated the thickness of the SiO_2 layer to be ∼0.4 nm and up to ∼1 nm for the as-grown and annealed samples in the saturated state, respectively.

Another interesting observation is the increase of the spectral weight in the range $E_B = -0 - -3$ eV upon irradiation [Fig. 4(a), insets] suggests generation of in-gap states in HfO_2 parallel to the generation of the V_Os. Following the general trend that the annealing greatly reduces the irradiation sensitivity of the samples, the evolution of the in-gap spectral weight is more pronounced for the as-grown samples than for the annealed ones.

Figures 4(d)–4(f) compile energies of the VB, Si $2p$, and Hf $5p$ spectral structures as a function of irradiation time for all studied samples. We note that in our measurements each 15-s-long acquisition was followed by 5 s to set up the next one; assuming a linear change of the spectrum during the acquisition time, the first spectrum corresponds to an irradiation time of 7.5 s, the next one to 27.5 s, etc. The VB and Hf $5p$ structures show monotonous downward energy shifts for all investigated samples, except for the annealed HfO_2/p^+Si one exhibiting a more complex behavior. The Si $2p$ spectra show a small downward shift for both HfO_2/n^+Si samples, an upward shift for the as-grown HfO_2/p^+Si sample, and again a nonmonotonous behavior upon annealing of the latter. As we discuss below, such nonmonotonous time dependence may indicate involvement of two competing processes, shifting the spectral peaks in opposite directions.

Finally, we note that the set of our experimental observations cannot entirely reconcile with the so-called "differential charging model" [20]. Firstly, the band bending in our HfO_2/p^+Si reduces under x-ray irradiation, whereas that model implies its buildup upon irradiation [20]. Secondly, we also observe that the Si $2p$ spectra of HfO_2/p^+Si strongly shift under irradiation. Moreover, there are nonmonotonic shifts of the Hf and Si core levels, which cannot be explained only by the charging. We conclude that the additional mechanism should be involved here, namely, the generation of (charged) oxygen vacancies in HfO_2 discussed below. It is intriguing to note that although the synchrotron x-ray radiation in our experiments delivered a photon density several orders of magnitude higher comparted to the x-ray tubes used in previous works, we have observed a similar timescale (several tens of minutes) of the electronic structure evolution. Such a hardness of our samples to x-ray irradiation might be connected with differences in the sample fabrication procedure or with low sample temperature in our experiments affecting the irradiation-induced physical process discussed below.

D. Role of V_Os in the irradiation-induced effects

The generation of V_Os under soft x-ray irradiation was previously observed and comprehensively studied for $SrTiO_3$ [44,45] and $LaAlO_3/SrTiO_3$ interfaces [46,47]. It was found that V_Os may generate via the Ti $3p$ core-hole Auger decay, and are located in close proximity of the $SrTiO_3$ surface (within ∼0.5 nm). Similar processes should occur under x-ray irradiation of HfO_2/Si. We conjecture that two processes are taking place: (1) the generation of V_Os at the surface of HfO_2 and at the interface with Si. Whereas the O atoms released at the surface escape to the vacuum, those at the interface, as we have seen above, react with Si to form SiO_2; and (2) charging of the created V_Os, which changes the $V(z)$ across HfO_2 and electronic band alignment at the HfO_2/Si interface. We note that while considering the redistribution of charges in HfO_2 under x-ray irradiation, we rule out either drift or diffusion of ions in HfO_2 since all measurements were performed at $T = 12$ K when any atomic motion is basically frozen. In any case, however, the electrons and holes in highly doped $n^+(p^+)$Si remain mobile, i.e., exhibit the metallic behavior [33].

The observed irradiation-induced downward shift of the VB and Hf $5p$ peak for HfO_2 [Figs. 4(a), 4(b), 4(d), and 4(e)] for the as-grown HfO_2/Si samples is suggestive of the generation of the V_O^+s in HfO_2 adjacent to Si in these samples and sample surface. At the same time, the diffusion and/or electromigration of charged V_Os from the interface into the bulk of HfO_2 can be ruled out owing to low temperature. The generation of the interfacial V_O^+s is consistent with the decrease of the band bending in Si evidenced by the sharpening of the Si $2p$ peak under irradiation. It is worth to note that the fitting of the spectra does *not* require a nonlinear potential distribution across HfO_2, which is another argument

supporting the conclusion that the charges are distributed only at its interfaces and not in its bulk.

The annealing of the HfO_2/p^+Si sample results in some oxidation of Si close to the interface and thus a lower V_O-generation rate under x-ray irradiation. However, V_Os on the HfO_2 surface may keep forming and charging, leading to a buildup of the potential drop across and band bending in the HfO_2 layer, as seen in the change of the shift of the HfO_2's VB and Hf $5p$ peak under irradiation from downward to upward [Figs. 4(d) and 4(e)]. At the same time, the band bending in Si decreases, as indicated in the narrowing of the Si $2p$ spectrum under irradiation [Fig. 4(c)]. The nonmonotonic shifts of the spectra [Figs. 4(d)–4(f)] may allow us to differentiate between the processes of (1) generation of V_Os on the HfO_2 surface, and (2) charging of the V_Os in HfO_2 at its surface and interface with Si, with the two processes having different rates. We conjecture that the process (1) comes first with x-ray irradiation, building the electric-dipole field in HfO_2, and driving the HfO_2's VB and Hf $5p$ peak downwards. Under further irradiation, the process (2) becomes dominant, shifting these spectral structures upwards. We can roughly estimate the characteristic time of V_O^+ generation under irradiation and subsequent recharging as several minutes and several tens of minutes, respectively.

Returning to HfO_2/n^+Si, the upward band bending in Fig. 3(c) should indicate negatively charged V_Os (V_O^-) at the surface of HfO_2. The excess of electrons would make the HfO_2 surface more susceptible to the x-ray irradiation, and in Figs. 4(d) and 4(e) we indeed observe a stronger time evolution of the VB and Hf $5p$ spectra compared to HfO_2/p^+Si. At the same time, neither the linewidth of the Si $2p$ doublet nor its E_B changes with time, indicating that the generation and charging of the surface V_O^-s do not affect the near-interface region of n^+Si. Upon annealing, the spectral features shift significantly less under x-ray irradiation [Fig. 3(d) and Figs. 4(c)–4(e)] for the same reasons as for the HfO_2/p^+Si.

E. Reconstruction of the band bending and built-in charges in pristine HfO_2/Si

Importantly, our time-evolution data have allowed us to quantify the extrinsic energy shifts of the VB and core-level spectral peaks caused by the x-ray irradiation, and correct the saturated offset values from Table I back to the intrinsic ones in the pristine samples. These true offset values for all studied samples are also included in Table I. The corresponding band diagrams are shown in Fig. 3 (green dashed lines) on top of those for the saturated state (black solid lines). For the HfO_2 region, this diagram was obtained by correcting the saturated-state potential with the observed temporal shift of the Hf $5p$ peak. For the Si region, we refitted the time-dependent Si $2p$ peaks in order to take into account their energy shifts due to band bending. We deem our experimental values of the band offsets locally at the HfO_2/Si interface to have a better accuracy compared to the previous works [20,21] where either the **k**-dispersion effects, band bending in both HfO_2 and Si, or the effects of x-ray irradiation were not taken into account.

In order to determine the exact values for the charges built up at both the HfO_2/Si interface and the HfO_2 surface, we further fit the derived band diagrams with the electrostatic model for the potential distribution across our HfO_2/n^+Si and HfO_2/p^+Si heterostructures using BSU BAND DIAGRAM program [48]. The results of the modeling shown in Fig. S7 in Ref. [34] perfectly match the experimentally derived band offset including the band bending and the width of the depletion regions in Si. The derived values for the surface and interface charges are also given in Fig. S7. In particular, the maximal surface charge we derived is $\sigma = 450\,\mu C/cm^2$ for the *in situ* annealed HfO_2/p^+Si sample. The interface charges are much smaller, on the order of several $\mu C/cm^2$, and for the as-grown HfO_2/n^+Si sample there was no interfacial charge at all within the accuracy of our fitting procedure.

It is worth noting that the modeling with BSU has required adjustment of the electron affinity of HfO_2 as a parameter in order to match the experimental results. This implies that the band gap in HfO_2 effectively varies depending on the type of the interface and heat treatment. These variations can be explained in terms of the defects generated in HfO_2, with the corresponding in-gap states lying within 1–1.5 eV below the conduction-band minimum. If the amount of such defects is large enough to form a continuous subband, the band gap effectively reduces. The electron affinity values used in the modeling ranged from $E_{ea} = 1.1$ eV for the annealed HfO_2/p^+Si sample to $E_{ea} = 3.35$ eV for the as-grown HfO_2/n^+Si one (see Fig. S5 in Ref. [34] for all values). These values correspond to the HfO_2 band gap $E_g = 5.4$ eV with the defect energy levels 1.5–2 eV below the conduction-band minimum [15,49].

IV. CONCLUSIONS

The electronic structure of ultrathin as-grown and *in situ* annealed HfO_2 films interfaced to highly doped (p^+ and n^+) Si has been studied using synchrotron-based x-ray photoelectron spectroscopy. Using angle-resolved measurements, **k**-resolved electronic structure $E(\mathbf{k})$ of the VB has been determined for the single-crystal Si substrate in contact with HfO_2, including the band offsets at the Γ point for both HfO_2/n^+Si and HfO_2/p^+Si interfaces. Furthermore, XPS of the Hf $4f$ and Si $2p$ core levels has allowed reconstruction of the band bending into Hf and Si from photon-energy dependent energies and line shapes of these spectral structures. Linear band bending in HfO_2 has indicated charges accumulated only at its surface and interface with Si. While the band bending into Si has been found almost flat for the HfO_2/n^+Si interfaces, it has been much stronger for the HfO_2/p^+Si ones. The effect of intense x-ray irradiation, used as a probe in our study, was evaluated from the time evolution of the experimental core-level and VB spectra. We have proposed a model explaining the observed evolution of the HfO_2/Si electronic structure under x-ray irradiation and heat treatment through release of O atoms and formation of V_Os at its surface and interface with Si. With the surface O atoms escaping into the vacuum and the interfacial ones reacting with Si to form a few monolayer thick SiO_2 layer at the interface, the V_Os left behind act as fixed surface and interface charges. Finally, the knowledge of the irradiation-dependent band bending at the HfO_2/Si interface has allowed most precise determination of the **k**-dependent

band offset locally at the HfO_2/Si interface in its pristine state.

ACKNOWLEDGMENTS

This work has been performed with the financial support from the Russian Science Foundation (Grant No. 18-12-00434-П) and University of Geneva as the Leading House for the Science and Technology cooperation program with Russia and the CIS Region. The processing of the experimental data obtained at SLS synchrotron was performed with the financial support by the Ministry of Science and Higher Education of the Russian Federation, Grant No. 075-11-2021-086. The samples have been fabricated and precharacterized using the equipment and with the help from the staff of the MIPT Center of Shared Facilities with partial financial support from the Ministry of Science and Higher Education of the Russian Federation (Agreement No. 075-00337-20-03, Project No. FSMG-2020-0001). We thank Dr. V. G. Valeyev for fruitful discussions.

[1] V. A. Gritsenko, T. V. Perevalov, and D. R. Islamov, Electronic properties of hafnium oxide: A contribution from defects and traps, Phys. Rep. **613**, 1 (2016).

[2] J. Robertson and R. M. Wallace, High-K materials and metal gates for CMOS applications, Mater. Sci. Eng. R **88**, 1 (2015).

[3] T. S. Böscke, J. Müller, D. Bräuhaus, U. Schröder, and U. Böttger, Ferroelectricity in hafnium oxide thin films, Appl. Phys. Lett. **99**, 102903 (2011).

[4] T. S. Böescke, J. Müller, D. Bräuhaus, U. Schröder, and U. Böttger, Ferroelectricity in Hafnium Oxide: CMOS Compatible Ferroelectric Field Effect Transistors, in *2011 IEEE International Electron Devices Meeting (IEDM), Washington, DC, USA* (IEEE, 2011), 24.5.1.

[5] S. Dünkel, M. Trentzsch, R. Richter, P. Moll, C. Fuchs, O. Gehring, M. Majer, S. Wittek, B. Müller, T. Melde *et al.*, A FeFET based super-low-power ultra-fast embedded NVM technology for 22nm FDSOI and beyond, in *2017 IEEE International Electron Devices Meeting (IEDM), San Francisco, CA, USA* (IEEE, 2017), 19.7.1.

[6] A. Chouprik, A. Chernikova, A. Markeev, V. Mikheev, D. Negrov, M. Spiridonov, S. Zarubin, and A. Zenkevich, Electron transport across ultrathin ferroelectric Hf0.5Zr0.5O2 films on Si, Microelectron. Eng. **178**, 250 (2017).

[7] V. Mikheev, A. Chouprik, Y. Lebedinskii, S. Zarubin, Y. Matveyev, E. Kondratyuk, M. G. Kozodaev, A. M. Markeev, A. Zenkevich, and D. Negrov, Ferroelectric second-order memristor, ACS Appl. Mater. Interfaces **11**, 32108 (2019).

[8] S. S. Cheema, N. Shanker, C. H. Hsu, A. Datar, J. Bae, D. Kwon, and S. Salahuddin, One nanometer HfO_2-based ferroelectric tunnel junctions on silicon, Adv. Electron. Mater. **8**, 2100499 (2022).

[9] M. Hoffmann, S. Slesazeck, and T. Mikolajick, Progress and future prospects of negative capacitance electronics: A materials perspective, APL Mater. **9**, 020902 (2021).

[10] G. Bersuker, D. C. Gilmer, D. Veksler, J. Yum, H. Park, S. Lian, L. Vandelli, A. Padovani, L. Larcher, K. McKenna *et al.*, Metal Oxide RRAM Switching Mechanism Based on Conductive Filament Microscopic Properties, in *2010 IEEE International Electron Devices Meeting (IEDM), San Francisco, CA, USA* (IEEE, 2010), 19.6.1.

[11] S. Yu, X. Guan, and H. S. P. Wong, Conduction mechanism of TiN/HfO_x/Pt resistive switching memory: A trap-assisted-tunneling model, Appl. Phys. Lett. **99**, 063507 (2011).

[12] Y. N. Tan, W. K. Chim, W. K. Choi, M. S. Joo, and B. J. Cho, Hafnium aluminum oxide as charge storage and blocking-oxide layers in SONOS-type nonvolatile memory for high-speed operation, IEEE Trans. Electron. Devices **53**, 654 (2006).

[13] E. P. Gusev, C. Cabral, M. Copel, C. D'Emic, and M. Gribelyuk, Ultrathin HfO_2 films grown on silicon by atomic layer deposition for advanced gate dielectrics applications, Microelectron. Eng. **69**, 145 (2003).

[14] *Defects in High-k Gate Dielectric Stacks: Nano-Electronic Semiconductor Devices*, edited by E. Gusev (Springer, Dordrecht, 2006).

[15] K. Xiong, J. Robertson, M. C. Gibson, and S. J. Clark, Defect energy levels in HfO_2 high-dielectric-constant gate oxide, Appl. Phys. Lett. **87**, 183505 (2005).

[16] S. Sayan, T. Emge, E. Garfunkel, X. Zhao, L. Wielunski, R. A. Bartynski, D. Vanderbilt, J. S. Suehle, S. Suzer, and M. Banaszak-Holl, Band alignment issues related to $HfO_2/SiO_2/p-Si$ gate stacks, J. Appl. Phys. **96**, 7485 (2004).

[17] A. Chernikova, M. Kozodaev, A. Markeev, D. Negrov, M. Spiridonov, S. Zarubin, O. Bak, P. Buragohain, H. Lu, E. Suvorova *et al.*, Ultrathin $Hf_{0.5}Zr_{0.5}O_2$ ferroelectric films on Si, ACS Appl. Mater. Interfaces **8**, 7232 (2016).

[18] Q. Li, S. J. Wang, K. B. Li, A. C. H. Huan, J. W. Chai, J. S. Pan, and C. K. Ong, Photoemission study of energy-band alignment for RuO_x/HfO_2/Si system, Appl. Phys. Lett. **85**, 6155 (2004).

[19] E. A. Kraut, R. W. Grant, J. R. Waldrop, and S. P. Kowalczyk, Semiconductor core-level to valence-band maximum binding-energy differences: Precise determination by x-ray photoelectron spectroscopy, Phys. Rev. B **28**, 1965 (1983).

[20] M. Perego and G. Seguini, Charging phenomena in dielectric/semiconductor heterostructures during x-ray photoelectron spectroscopy measurements, J. Appl. Phys. **110**, 053711 (2011).

[21] E. Bersch, M. Di, S. Consiglio, R. D. Clark, G. J. Leusink, and A. C. Diebold, Complete band offset characterization of the HfO_2/SiO_2/Si stack using charge corrected x-ray photoelectron spectroscopy, J. Appl. Phys. **107**, 043702 (2010).

[22] R. Puthenkovilakam and J. P. Chang, An accurate determination of barrier heights at the HfO_2/si interface *s*, J. Appl. Phys. **96**, 2701 (2004).

[23] L. Q. Zhu, N. Barrett, P. gou, F. Martin, C. Leroux, E. Martinez, H. Grampeix, O. Renault, and A. Chabli, X-Ray photoelectron spectroscopy and ultraviolet photoelectron spectroscopy investigation of Al-related dipole at the HfO_2/Si interface, J. Appl. Phys. **105**, 024102 (2009).

[24] C. J. Yim, D. H. Ko, M. H. Jang, K. B. Chung, M. H. Cho, and H. T. Jeon, Change in band alignment of HfO_2 films with annealing treatments, Appl. Phys. Lett. **92**, 012922 (2008).

[25] A. Damascelli, Z. Hussain, and Z. X. Shen, Angle-resolved photoemission studies of the cuprate superconductors, Rev. Mod. Phys. **75**, 473 (2003).

[26] V. N. Strocov, L. L. Lev, M. Kobayashi, C. Cancellieri, M. A. Husanu, A. Chikina, N. B. M. Schröter, X. Wang, J. A. Krieger, and Z. Salman, *K*-resolved electronic structure of buried heterostructure and impurity systems by soft-x-ray ARPES, J. Electron Spectrosc. Relat. Phenom. **236**, 1 (2019).

[27] V. N. Strocov, M. Kobayashi, X. Wang, L. L. Lev, J. Krempasky, V. V. Rogalev, T. Schmitt, C. Cancellieri, and M. L. Reinle-Schmitt, Soft-x-ray ARPES at the Swiss Light Source: From 3D materials to buried interfaces and impurities, Synchrotron Radiat. News **27**, 31 (2014).

[28] L. L. Lev, D. v. Averyanov, A. M. Tokmachev, F. Bisti, V. A. Rogalev, V. N. Strocov, and V. G. Storchak, Band structure of the EuO/Si interface: Justification for silicon spintronics, J. Mater. Chem. C **5**, 192 (2016).

[29] L. L. Lev, I. O. Maiboroda, M.-A. Husanu, E. S. Grichuk, N. K. Chumakov, I. S. Ezubchenko, I. A. Chernykh, X. Wang, B. Tobler, T. Schmitt *et al.*, *K*-space imaging of anisotropic 2D electron gas in GaN/GaAlN high-electron-mobility transistor heterostructures, Nat. Commun. **9**, 2653 (2018).

[30] C. Cancellieri, A. S. Mishchenko, U. Aschauer, A. Filippetti, C. Faber, O. S. Bariši, V. A. Rogalev, T. Schmitt, N. Nagaosa, and V. N. Strocov, Polaronic metal state at the $LaAlO_3/SrTiO_3$ interface, Nat. Commun. **7**, 10386 (2016).

[31] T. Yu, J. Wright, G. Khalsa, B. Pamuk, C. S. Chang, Y. Matveyev, X. Wang, T. Schmitt, D. Feng, D. A. Muller *et al.*, Momentum-resolved electronic structure and band offsets in an epitaxial NbN/GaN superconductor/semiconductor heterojunction, Sci. Adv. **7**, 5833 (2021).

[32] L. L. Lev, I. O. Maiboroda, E. S. Grichuk, N. K. Chumakov, N. B. M. Schröter, M.-A. Husanu, T. Schmitt, G. Aeppli, M. L. Zanaveskin, V. G. Valeyev, and V. N. Strocov, Impact of Band-Bending on the *k*-Resolved Electronic Structure of Si-Doped GaN, Phys. Rev. Research **4**, 013183 (2022).

[33] C. Yamanouchi, K. Mizuguchi, and W. Sasaki, Electric conduction in phosphorus doped silicon at low temperatures, J. Phys. Soc. Jpn. **22**, 859 (2013).

[34] See Supplemental Material at http://link.aps.org/supplemental/10.1103/PhysRevMaterials.6.084605 for the Si 2p core-level spectra measured by the laboratory XPS prior to the HfO_2 growth; raw ARPES image for a HfO_2/p^+Si as-grown sample; valence-band offset evaluation example; $h\nu$ dependence of the Si $2p$ and Hf $4f$ core-level spectra; effect of band bending on broadening of the core-level spectra; O $1s$ core-level spectra; evolution of spectra with irradiation dose; the model of the potential distributions across the HfO_2/Si stacks; calculations of the potential distribution in Si and HfO_2; a table of the Si $2p$ and Hf $4f$ full widths at half maximum.

[35] J. J. Yeh and I. Lindau, Atomic subshell photoionization cross sections and asymmetry parameters: $1 \leqslant Z \leqslant 103$, At. Data Nucl. Data Tables **32**, 1 (1985).

[36] J. Braun, J. Minár, S. Mankovsky, V. N. Strocov, N. B. Brookes, L. Plucinski, C. M. Schneider, C. S. Fadley, and H. Ebert, Exploring the XPS limit in soft and hard x-ray angle-resolved photoemission using a temperature-dependent one-step theory, Phys. Rev. B: Condens. Matter Mater. Phys. **88**, 205409 (2013).

[37] C. J. Powell and A. Jablonski, *NIST Electron Inelastic-Mean-Free-Path Database, Version 1.2* (National Institute of Standards and Technology, Gaithersburg, MD, 2010).

[38] V. N. Strocov, Intrinsic accuracy in 3-dimensional photoemission band mapping, J. Electron Spectrosc. Relat. Phenom. **130**, 65 (2003).

[39] J. Robertson, O. Sharia, and A. A. Demkov, Fermi level pinning by defects in HfO_2-metal gate stacks, Appl. Phys. Lett. **91**, 132912 (2007).

[40] A. Zenkevich, Y. Lebedinskii, M. Pushkin, and V. Nevolin, Surface electronic structure of HfO_2 resolved with low energy ion spectroscopy, Appl. Phys. Lett. **89**, 172903 (2006).

[41] M. Grundmann, *The Physics of Semiconductors: An Introduction Including Nanophysics and Applications*, 4th ed. (Springer, Cham, Switzerland, 2021).

[42] S. Ristic, A. Prijic, and Z. Prijic, Dependence of static dielectric constant of silicon on resistivity at room temperature, Serb. J. Elect. Eng. **1**, 237 (2004).

[43] S. Tanuma, C. J. Powell, and D. R. Penn, Calculations of electron inelastic mean free paths for 31 materials, Surf. Interface Anal. **11**, 577 (1988).

[44] S. M. Walker, F. Y. Bruno, Z. Wang, A. de la Torre, S. Riccó, A. Tamai, T. K. Kim, M. Hoesch, M. Shi, M. S. Bahramy *et al.*, Carrier-density control of the $SrTiO_3$ (001) surface 2D electron gas studied by ARPES, Adv. Mater. **27**, 3894 (2015).

[45] L. Dudy, M. Sing, P. Scheiderer, J. D. Denlinger, P. Schütz, J. Gabel, M. Buchwald, C. Schlueter, T. L. Lee, and R. Claessen, In situ control of separate electronic phases on $SrTiO_3$ Surfaces by oxygen dosing, Adv. Mater. **28**, 7443 (2016).

[46] V. N. Strocov, A. Chikina, M. Caputo, M. A. Husanu, F. Bisti, D. Bracher, T. Schmitt, F. Miletto Granozio, C. A. F. Vaz, and F. Lechermann, Electronic phase separation at $LaAlO_3/SrTiO_3$ interfaces tunable by oxygen deficiency, Phys. Rev. Mater. **3**, 106001 (2019).

[47] V. N. Strocov, F. Lechermann, A. Chikina, F. Alarab, L. L. Lev, V. A. Rogalev, T. Schmitt, and M.-A. Husanu, Dimensionality of mobile electrons at x-ray-irradiated $LaAlO_3/SrTiO_3$ interfaces, Electron. Struct. **4**, 015003 (2022).

[48] R. G. Southwick, A. Sup, A. Jain, and W. B. Knowlton, An interactive simulation tool for complex multilayer dielectric devices, IEEE Trans. Device Mater. Reliab. **11**, 236 (2011).

[49] S. Monaghan, P. K. Hurley, K. Cherkaoui, M. A. Negara, and A. Schenk, Determination of electron effective mass and electron affinity in HfO_2 using MOS and MOSFET structures, Solid State Electron. **53**, 438 (2009).